The MEASUREMENTS AND ANALYSIS OF CORE LOSSES FOR A 4kW BEARINGLESS PERMANENT MAGNET SLICE MOTOR

Huangqiu Zhu
Jiangsu University, School of Electrical
and Informational Engineering, 212013 Zhenjiang, China
zhuhuangqiu@ujs.edu.cn
Pascal N. Boesch
Swiss Federal Institute of Technology (ETH), Laboratory
for Electrical Engineering Design (EEK), 8092 Zurich, Switzerland
boesch@eek.ee.ethz.ch

ABSTRACT

As bearingless motors have all advantages of magnetic bearings, they play an important role in solving difficult problems of electric drives. The simplest and most versatile form of bearingless motor is the bearingless slice motor. When the rotor, which carries an impeller and is levitated within the hermetically closed pump housing, turns with a high rotational speed, liquid is pumped from the inlet to the outlet. This type of magnetically levitated centrifugal pump system has a wide range of applications like in life science, chemical processing industry, semiconductor manufacturing industry, foodstuff processing industry and so on. The technology of small power bearingless slice motors is already mature and bearingless pump systems have been applied in industries. However no bearingless slice motors over 1.2kW have been produced. In this paper, a system of bearingless permanent magnet slice motors is introduced; a 3-phase permanent magnet slice motor with the power around 4kW is set up; theoretical formulas of core losses in bearingless motors are introduced and the core losses are investigated. Based on experiments and analysis, it has been found that choosing an appropriate permanent magnetic rotor, a back iron, and appropriate isolation between iron cores and a back iron can reduce core losses of the motor. And core losses account for only about 3~4% of total power, when the bearingless permanent magnet slice motor works at rating speed 7 700rpm.

INTRODUCTION

Bearingless motor does not mean the lack of bearing forces, which are necessary in any case to stabilize the rotor, but the missing of physical contact bearing components. The principle of the bearingless motor is based on the contactless magnetic bearing of the rotor. Contrast to conventional magnetic levitated drives, the bearing forces in the bearingless motor are not built up in separated magnetic bearings, which are placed on the left- and right-hand side of the motor block, but in the motor itself [1,2,3].

As bearingless motors have all advantages of magnetic bearings, such as no mechanical contact, no wearing, no need of lubrication, no pollution and long service life, they play an important role in solving difficult problems of electric drives. The simplest and most versatile form of bearingless motor is bearingless slice motor. When the length of the rotor is small compared to the diameter, 3 degrees of freedom can be stabilized passively. The remaining 3 degrees of freedom are controlled actively [3,4,5]. First, radial forces are controlled by the current in bearing windings. Second, torque is controlled by the current in driving windings. When the rotor, which carries an impeller and is levitated within the hermetically closed pump housing, turns with a high rotational speed, liquid is pumped from the inlet to the outlet. This type of magnetically levitated centrifugal pump system has a wide range of applications like in scopes of life science [3], chemical processing industry [4], semiconductor manufacturing industry [4,5], foodstuff processing industry and so on. The technology of small power bearingless slice motors is already mature and bearingless pump systems have been applied in industries. However no motors over 1.2kW have been produced. In this paper, the 3-phase permanent magnet slice motor with the power around 4kW is set up, theoretical formulas of bearingless motors are introduced and the motor losses are investigated mainly on the core losses. Based on the experiments, reduction of power losses can be achieved by choosing an appropriate permanent magnetic rotor, a back irons and so on.

SYSTEM OVERVIEW

As shown in FIGURE 1, the system of bearingless permanent magnet slice motor consists of a motor, power-board, DSP-board, sensors, and RS232 interface. The motor consists of stator iron cores, stator back iron, permanent magnet rotor, bearing winding, and driving winding. There is one pole pair of permanent magnet rotor and two pole pair of bearing fields. The two sets of windings are designed to be a 3-phase symmetrical structure. The central processing unit (CPU) used in DSP-board is digital signal processor (DSP) TMS320F240. Its timing frequency is 20MHz, and it has 12 compare/pulse-width modulation (PWM) channels, 16 dual 10-bit A/D conversion modules. The instruction cycle time is 50 ns. The DSP system collects the signals of rotor positions and speed, and output PWM signal to control the bearing winding and the driving winding.

The outputs of sensors are sent to DSP-board. The RS232 interface communicates between DSP-board and a computer. The control parameters can be adjusted by a computer with special debugging software designed by Levitronix Company in Switzerland. The bearingless permanent magnet slice motor is controlled by directional control of the rotor magnetic field.

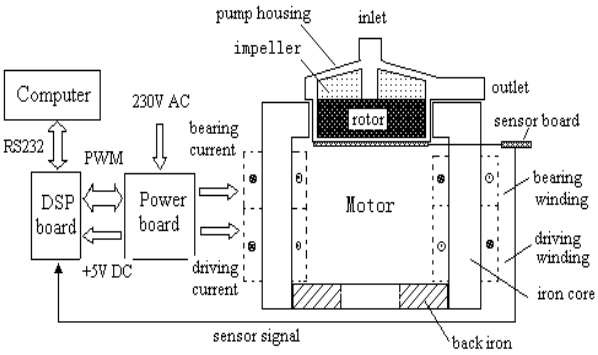

FIGURE 1: Sketch of bearingless slice motors

SKECH OF CONTROL SYSTEM

FIGURE 2 shows the system configuration of the permanent magnet slice motor. In the motor speed controller, the rotational angular speed ω_m is detected by the Hall sensors. The Proportional-Integral (PI) motor speed controller generates the q-coordinate current command $i_{1q}^{(F)*}$ in the rotor coordinates. The d-coordinate current command $i_{1d}^{(F)*}$ in the rotor coordinates equals zero. The 2-phase practical current $i_{1u}^{(S)}$ and $i_{1v}^{(S)}$ in the stator coordinates are measured by current sensors. After accounting the w-phase current $i_{1w}^{(S)}$, the 3-phase motor practical current $i_{1u}^{(S)}$, $i_{1v}^{(S)}$ and $i_{1w}^{(S)}$ are transformed from 3-phase to 2-phase, then transformed into practical current $i_{1d}^{(F)}$ and $i_{1q}^{(F)}$ in the rotor coordinates. The current commands $i_{1d}^{(F)*}$ and $i_{1q}^{(F)*}$ are compared to practical current $i_{1d}^{(F)}$ and $i_{1q}^{(F)}$, then differences are amplified by PI motor current controllers. The 2-phase motor voltage command $u_{1d}^{(F)*}$ and $u_{1q}^{(F)*}$ in the rotor coordinates are transformed into motor voltage command $u_{1d}^{(S)*}$ and $u_{1d}^{(S)*}$ in the stator coordinates, and then transformed from 2-phase to 3-phase. The 3-phase motor voltage commands $u_{1u}^{(S)*}$, $u_{1v}^{(S)*}$ and $u_{1w}^{(S)*}$ are modulated by PWM, then amplified by IGBT-modules, and at last motor winding voltages $u_{1u}^{(S)}$, $u_{1v}^{(S)}$ and $u_{1w}^{(S)}$ are generated. In FIGURE 3, the angel φ_D is the preliminary angel of motor winding in the stator coordinates.

Rotor shaft displacements in X and Y directions are detected by eddy current sensors. These displacements are compared to references X^* and Y^*, then the differences are adjusted by Proportional-integral-derivative (PID) controllers, and the radial force current commands $i_{2d}^{(F)*}$ and $i_{2q}^{(F)*}$ in the rotor coordinates are generated. The bearing winding voltages $u_{1u}^{(S)}$, $u_{1v}^{(S)}$ and $u_{1w}^{(S)}$ are generated like control part of the motor winding. In FIGURE 2, the angel φ_B is the preliminary angel of the bearing winding in the stator coordinates.

FORMULAS OF CORE LOSSES

The total motor losses at no load consist of the copper losses and the core losses. In this study only core losses are considered. The total core loss consists of the eddy current losses and the hysteresis losses with equation (1). If the magnetic flux density has a homogenous distribution and a sinusoidal time behavior, the eddy current losses in iron laminations can be calculated approximately with equation (2). For iron and for a magnetic flux density between 0.2 and 1.5T equation. Equation (3) describes the hysteresis losses.

$$P_{Fe} = P_{FeE} + P_{FeH} \qquad (1)$$

P_{Fe} __ total core losses;

P_{FeE} __eddy losses;

P_{FeH} __ hysteresis losses.

$$\begin{cases} P_{FeE} = c_{FeE} \cdot f_B^2 \cdot \hat{B}^2 \cdot e_{Fe}^2 \cdot m_{Fe} \\ m_{Fe} = V_{Fe} \cdot \delta_{Fe} \end{cases} \qquad (2)$$

c_{FeE} __material constant of the eddy current losses;

f_B ___frequency of the magnetic flux density;

$\hat{B}$ ___amplitude value of the magnetic flux density;

m_{Fe} ___mass of the used iron;

V_{Fe} ___volume of the used iron;

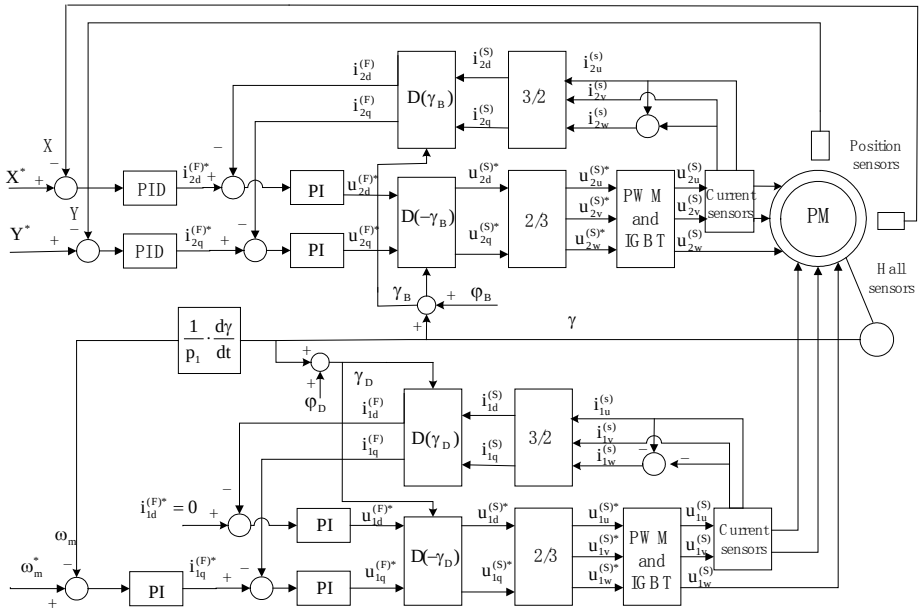

FIGURE2: Sketch of control system for the bearingless permanent magnetic slice motor

δ_{Fe} ___Specific gravity of the used iron;

e_{Fe} ___ lamination thickness.

$$P_{FeH} = c_{FeH} \cdot f_B \cdot \hat{B}^{1.6} \cdot m_{Fe} \qquad (3)$$

c_{FeH} ___material constant of the hysteresis losses.

In the PM-synchronous slice motor, the magnetic flux density is mainly generated by the permanent magnet rotor. The flux generated by the coils of the drive winding and the bearing winding can be ignored. The frequency of the magnetic flux density depends on the rotor speed and can therefore be calculated according to equation (4):

$$f_B = p_1 \cdot \frac{1}{2\pi} \cdot \omega_m \qquad (4)$$

The eddy current losses increase with the square of the speed and the hysteresis losses are proportional to the rotor speed. The core losses increase with a stronger magnet (for the same amount of iron).

MEASUREMENTS AND RESULTS

The ideal is to decrease the power losses of permanent magnetic slice motor. The experiments have been carried through two kinds of rotors with different parameters (TABLE 1), two kinds of back irons (FIGURE 3, TABLE 2) made of silicon irons with different configurations or thickness, two kinds of methods connecting between iron corns and back iron. The purpose is to design an optimal rotor, an optimal configuration of the back iron. The parameters of rotors are shown in TABLE 1. The parameters of back irons of silicon irons with different configurations are shown in TABLE 2.

TABLE 1: Parameters of rotors

Rotor	Thickness (mm)	Outside Diameter (mm)	Inner Diameter (mm)	Residual magnetic induction B_r(T)
HR510	20	80	30	1.2~1.3
HR633	25	78	30	1.3~1.4

TABLE 2: Parameters of back irons

The name of back irons of silicon iron	Thickness of each lamination (mm)	Outside diameter (mm)	Inner diameter (mm)
Keeper1	0.5mm	168	70
Keeper2	0.5mm	122	70

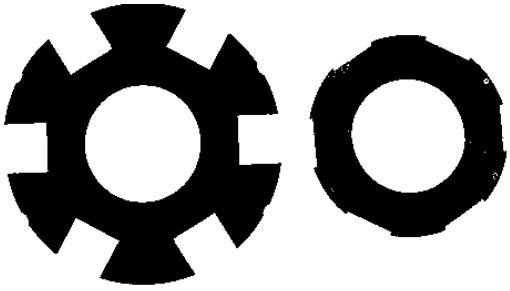

FIGURE3: Two kinds of back irons

The experiments have been measured at no load. Through measuring currents of driving windings,

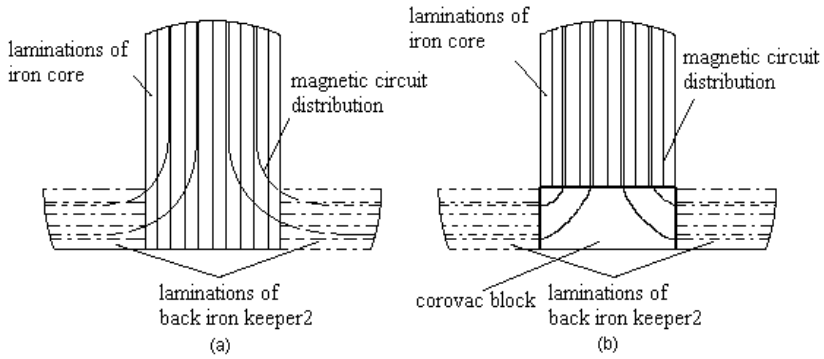

FIGURE5: Magnetic circuit distributions between iron core and back iron

induced voltage in the drive winding, and the core losses can be worked out.

According to formulas (1) ~ (4), the total core losses will increase mostly in conic when the magnetic induction in air gap is enhanced, and will increase completely in conic when the speed of the motor goes up. For two kinds of rotors, the back iron Keeper1 with 20mm is adopted. The curves of core losses are shown in FIGURE 4. As shown in FIGURE 4, the core losses will increase as the speed of the motor increases; and the core losses of the rotor HR633 is higher than the rotor HR510.

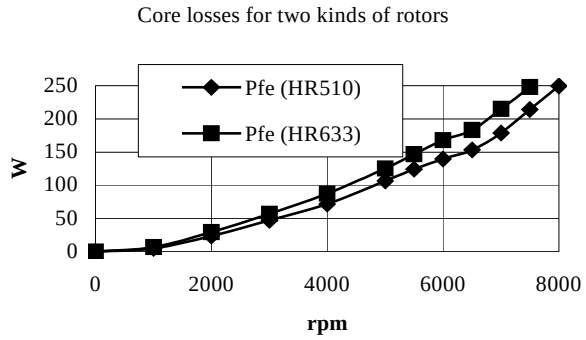

FIGURE4: Core losses for two kinds of rotors

FIGURE 5 shows that magnetic circuits distribute between iron core and back iron keeper1 and keeper2. Referencing FIGURE 3 and FIGURE 5, each tooth of keeper1 has 3 joint surfaces, which is 1 face and 2-side face with each iron core. Each tooth of keeper2 has only 1 joint face. The magnetic circuits in keeper2 are outspreaded in the directions of iron core's nearside and starboard. FIGURE 5(b) shows that magnetic circuits come into the back iron from the iron core without threading the laminations of the iron core. However in FIGURE 5(a) the part magnetic circuits vertically go into back iron keeper1 from 2 sides of the iron core through the laminations of the iron core. Therefore this situation brings additional eddy current losses. In addition, the 2 side faces of the iron core also bring short circuits between the laminations of back iron keeper1, and the short circuits also produce additional eddy current losses in the back iron.

For the rotor HR510, the two kinds of back irons with different configurations are used, and the thickness of these two kinds of back irons is 20mm. The core losses of keeper1 and keeper2 are shown in FIGURE 6. The curves have shown that the core losses with the back iron keeper1 are higher than that of the back iron keeper2 at the same speed.

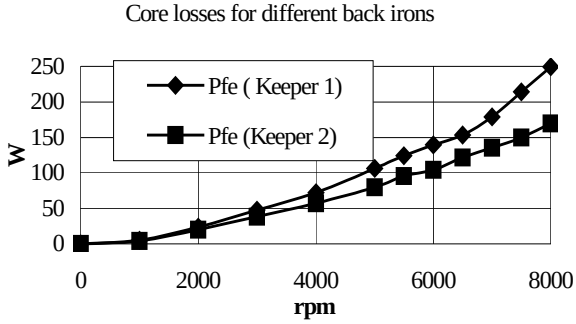

FIGURE6: Core losses for two kinds of different back irons

According to the formulas (2) and (3), the core losses of back irons will change as the varieties of magnetic induction in back irons and the mass of back irons. As the other parameters don't change, the core losses of back irons will change in inverse ratio with the change of the thickness of the back iron. Therefore total core losses inclusive back irons and iron cores will increase as the descending of the thickness of the back irons.

In experiments, the rotor HR510 is used. When the speed of the motor is at 3 000rpm or at 6 000rpm, the data are measured. The core losses will decrease as the thickness of keeper2 is added, as shown in FIGURE 7.

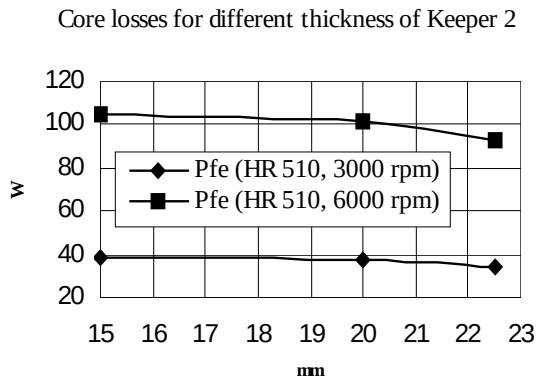

FIGURE7: Core losses for different thickness of the back iron

For decreasing the eddy current losses, back irons and iron cores usually consist of many isolation laminations. The basic configuration of iron core and back iron has been shown in FIGURE1 and FIGURE3. When iron cores are connected with back irons, laminations of iron cores and back iron bring on short circuits each other. Therefore, using isolation between iron cores and the back iron, short circuits will be avoided, and the eddy current losses of iron cores and back iron will decrease a little. For the rotor HR510, the thickness 17.5mm of keeper2 is used. When considering isolation between the core irons and the back irons, a simple method is using isolation paper. As shown in FIGURE 8, the core losses are smaller than the core losses without isolation.

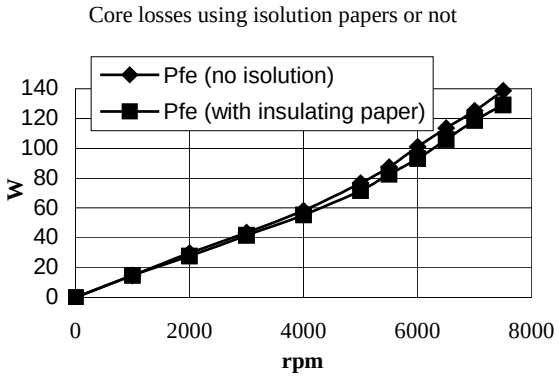

FIGURE8: Core losses using isolation papers or not

In FIGURE 5(b), when the magnetic field go into the back iron, the lines of magnetic forces must turn vertically in laminations of iron cores and go into laminations of the back iron. This vertical magnetic field also produces additional eddy current losses. In upper section , the data have been measured with isolation papers between core irons and back irons. As shown in FIGURE 9 blocks made from corovac material are used, and can insure insulation between iron cores and back irons. As the resistively of the material corovac is very high compared to ferrite cores, the vertical magnetic field in corovac almost doesn't produce eddy losses. As shown in FIGURE 10, for the rotor HR510, the core losses with corovac blocks are smaller than the core losses with isolation papers when the other parameters are the same.

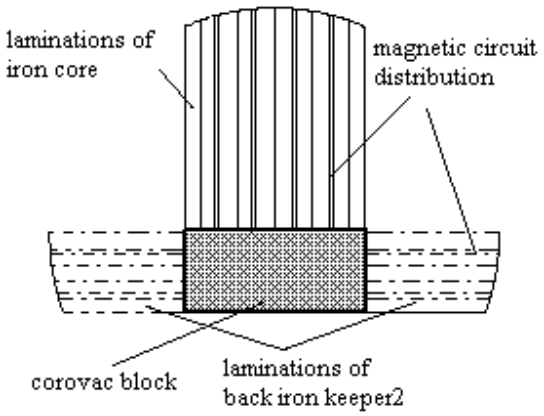

FIGURE 9: Connection between iron core and back iron with corovac block

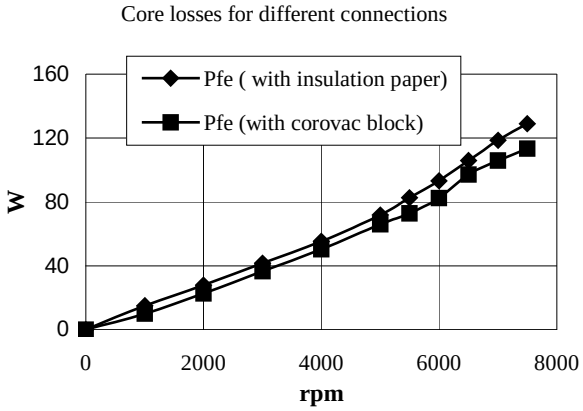

FIGURE10: Core losses connecting between iron core and back iron with corovac blocks

SUMMARY AND CONCLUSION

Based on analyzing and experiments about core losses of a bearingless permanent magnet slice motor, and considering total configuration and performance synthetically, using the rotor HR510, back iron keeper2 and isolation papers between the back iron and iron core, can produce optimal results. Core losses are small under this selection with core losses counting about 3 ~

4% of total power, when the permanent magnetic slice motor works at rating speed 7 700rpm.

ACKNOWLEDGEMENT

The project was supported by the Laboratory of Electrical Engineering Design (EEK) of Swiss Federal Institute of Technology (ETH) in Zurich and Levitronix GmbH in Zurich. The project was also sponsored by the National Natural Science Foundation of China (50275067) and SRF for ROCS, SEM and so on.

The author worked as visiting scholar instructed by professor J. Hugel at Swiss Federal Institute of Technology from November 2002 to November 2003.

REFERENCES

[1] Salazar A., Chiba A., Fukao T., A Review of Developments in Bearingless Motors, Proc. of the 7th International Symposium on Magnetic Bearings, Zuerich, Switzerland, 2000

[2] Bichsel J., Beitraege zum Lagerlosen Elektromotor, Dissertation ETH Zuerich, 1990

[3] Barletta N., Der lagerlose Scheibenmotor, Dissertation ETH Zuerich, 1998

[4] Neff M., Barletta N., Schoeb R., Bearingless Centrifugal Pump for Highly Pure Chemicals, Proc. Of the 8th International Symposium on Magnetic Bearing, Mito, Japan, 2002

[5] Neff M., Magnetgelagertes Pumpsystem fuer die Halbleiterfertigung, Dissertation ETH Zuerich, 2003